RESEARCH ARTICLE

WILEY

A multiaxial inertial macroelement for bridge abutments

Davide Noè Gorini[1] (ORCID) | **Luigi Callisto**[1] | **Andrew J. Whittle**[2] | **Salvatore Sessa**[3]

[1]Sapienza University of Rome, Rome, Italy

[2]Massachusetts Institute of Technology, Cambridge, Massachusetts, USA

[3]University of Naples Federico II, Naples, Italy

Correspondence
Davide Noè Gorini, Department of Structural and Geotechnical Engineering, via Eudossiana 18, Roma 00184, Italy.
Email: davideno.gorini@uniroma1.it

Funding information
Italian Department of Civil Protection, Grant/Award Number: ReLUIS-DPC 2019–2021

Abstract

This paper proposes a multiaxial macroelement for bridge abutments that can be included in the global structural model of a bridge to carry out nonlinear dynamic analyses with very much smaller computational effort than can be achieved using continuum representations of embankment and foundation soil behaviour. The proposed macroelement derives a constitutive force–displacement relationship within a rigorous thermodynamic framework and includes important features of non-linearity and directional coupling in characterizing the interactions of the abutment with the soil. In a dynamic analysis, the frequency-dependent response of the system is simulated through the combination of the macroelement with appropriate participating masses. The calibration procedure of the macroelement is based on the assessment of its ultimate capacity and of its response at small displacements, and it is shown that these ingredients can be derived through standardised procedures. In the paper, the macroelement response is validated against the results of fully coupled continuum numerical analyses for a reference soil–abutment system, under both static and seismic loading conditions. We show that the two models achieve similar predictions of maximum and permanent abutment deformations (less than 10–14% difference, respectively) for a suite of three-axis seismic loading events.

KEYWORDS
hyper-plasticity, inertial effects, macroelement, OpenSees, soil–abutment interaction

1 | INTRODUCTION

During a seismic event, a bridge abutment shows an intermediate behaviour between a retaining structure and a foundation. The abutment receives dynamic actions from both the soil and the bridge superstructure, with a significant exchange of inertial forces due to the large soil mass involved in the overall response.[1] These inertial effects are primarily caused by the dynamic participation of the approach embankment, which tends to control the frequency-dependent response of the soil–abutment system.[1–3] The dynamic amplification of the abutment response calls into play the nonlinear behaviour of the surrounding soil, causing permanent displacements and internal forces in the structural members of the bridge

during strong shaking.[4,5] However, the dynamic amplification of the forces transferred to the deck is limited by the ultimate capacity of the soil–abutment system, that depends strongly on the load direction.[6,7]

Nonlinear dynamic analysis is rapidly becoming a common means for seismic assessment of existing structures exhibiting highly nonlinear features. In this context, the plasticity-based macroelements[1,8–11] represent a promising approach to characterize realistically the soil–structure interaction effects within dynamic structural analyses, that can be accomplished with manageable computational effort. In prior research for bridge abutments, Shamsabadi et al.[12,13] developed a hyperbolic model to reproduce the progressive mobilisation of the passive resistance in the soil fill under monotonic, uniaxial loading conditions. More recently, Gorini et al.[1] developed a one-dimensional macroelement of the soil–abutment system (1D SAME) within a rigorous thermodynamic framework to simulate the combined nonlinear and inertial response exhibited by bridge abutments under dynamic loading. The 1D SAME was then validated under uniaxial loading, demonstrating the central role of the overall dynamic response of the abutments on the bridge performance.

In this paper we propose the multiaxial generalisation of the macroelement proposed by Gorini et al.[1] to simulate the monotonic and dynamic response of bridge abutments under general loading. A comprehensive description of the novel aspects of the proposed thermodynamic formulation is provided. A detailed derivation of the incremental response and of its identification is then presented for a direct implementation in numerical analyses of bridges. Finally, the macroelement is validated against the results of static and dynamic analyses for a reference, fully coupled soil–abutment numerical model, inspired by a well-documented case study.

2 | FORMULATION OF THE MACROELEMENT

2.1 | Conceptual framework

The proposed inertial macroelement, called SAME, is conceived as a multiaxial, nonlinear relationship between the interaction forces, Q_i, exchanged at the deck–abutment contact and the corresponding displacements, q_j, simulating the response of the abutment and of the large volume of soil interacting with it (foundation soil and approach embankment). The incremental force–displacement relationship reads:

$$\dot{Q}_i = H_{ij}, \dot{q}, \ i = 1, 2, 3; \ j = 1, 2, 3 \tag{1}$$

in which H_{ij} is the second-order tangent stiffness matrix, whose components represent the force in the i-direction produced by a unit displacement along the j direction. Here, the focus is on semi-integral abutments (hinged bearing devices supporting the deck) for which moment transmission on the abutment top can be reasonably neglected.[6,11] The formulation is accordingly restricted to the three translational degrees of freedom of the deck–abutment contact, corresponding to the longitudinal, transverse, and vertical directions of the bridge, named axes 1, 2, and 3, respectively.

The macroelement was formulated as a multi-surface plasticity model with kinematic hardening derived within a rigorous thermodynamic framework, using hyper-plasticity,[14] that ensures the consistency of deformation processes. In this manner, the macroelement response is completely defined through the specification of two potentials, namely the energy and dissipation functions. Hence, the tangent stiffness matrix in Equation (1) can be derived by differentiating the potentials. The potential functions were determined to incorporate three essential features of the response of bridge abutments: (i) material nonlinearity; (ii) load directional dependent response; and (iii) evolution of the nonlinear response with the level of mobilised strength in the soil through a thermodynamic-based kinematic hardening law.

The dissipative response of the macroelement was formulated on the basis on some primary assumptions, that are the validity of the orthogonality principle,[15] the additive decomposition of the elastic and plastic components of deformations and the associativity of the plastic flows.

2.2 | Plastic domain

In the context of multi-surface plasticity, the plastic domain of the macroelement is constituted by N yield surfaces in the space of the interaction forces at the deck–abutment contact within which the model exhibits an elastic–plastic, hardening response. The plastic response activates in correspondence of the surface of first yield ($n = 1$), within which the response is linear elastic, and is bounded by the surface of ultimate loads ($n = N$).
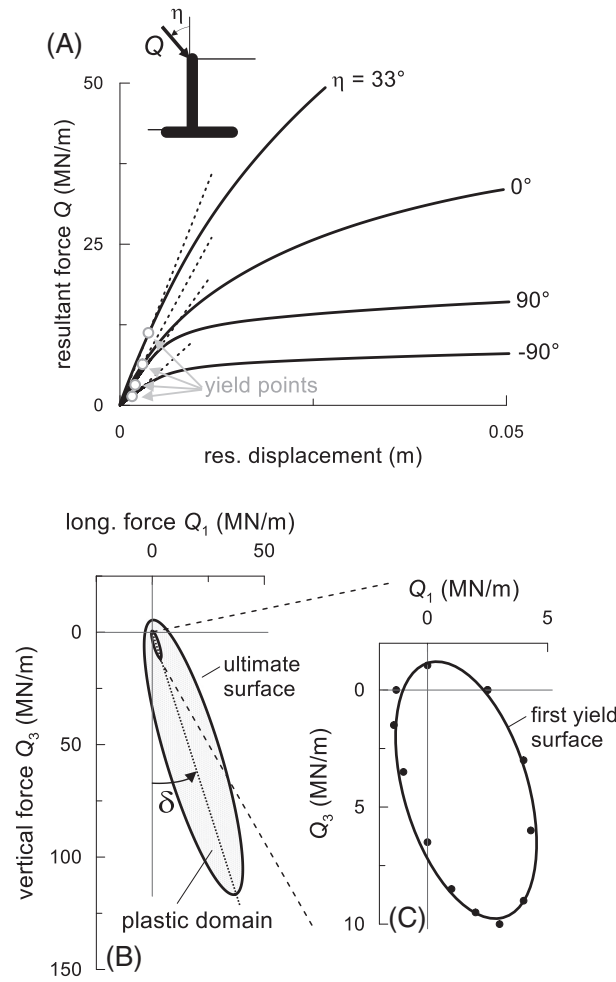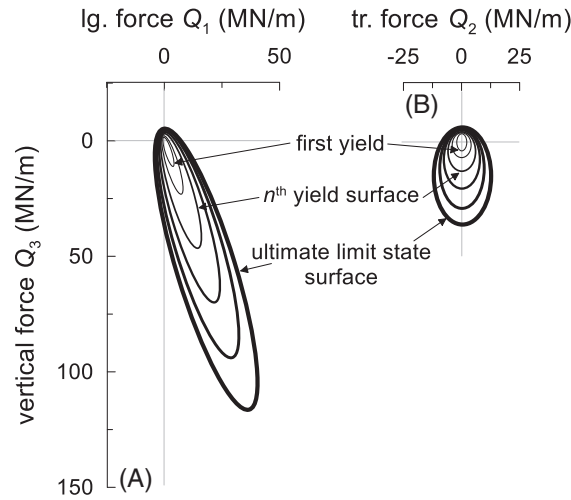
FIGURE 1 (A) Pushover curves obtained with the soil–abutment model developed in Gorini et al.[3] for different directions of the load, Q, applied to the abutment top; traces of the (B) ultimate and (C) first yield surfaces of the macroelement in the Q_1–Q_3 force space

For instance, Figure 1A illustrates the longitudinal response of the abutment to an inclined deck load (with longitudinal and vertical force components, Q_1 and Q_3, respectively). The shape and size of the innermost yield surface (Figure 1C), $y^{(1)}$, were studied through static finite-element analyses of soil–abutment systems (Figure 1A; cf. Gorini et al.[3]; Gorini[11]). Hence, $y^{(1)}$ is regarded as the locus in the force space associated with significant changes of the force–displacement relationships with respect to the small-strain response. The ultimate yield surface, $y^{(N)}$, Figure 1B, represents the force combinations activating global plastic mechanisms of the soil–abutment system and is described by the relationship proposed by Gorini et al.[6] The ultimate surface forms an ellipsoidal locus in the force space decentred from the axis origin, as an effect of the highly asymmetry in the abutment response, and rotated of an angle δ with respect to the Q_3-axis. Although the case illustrated in Figure 1 refers to an abutment with a shallow foundation, a recent study demonstrated that a similar roto-translated ellipsoidal shape can be adopted in the case of abutments with deep foundations as well.[7]

It can be observed that these first yield and ultimate surfaces can be taken as homothetic to each other. The remaining yield surfaces were then assumed to be all homothetic to the ultimate surface, as shown in Figure 2, such that the analytical expression of the nth yield surface is given by:

$$y^{(n)} = \frac{\left[\left(Q_1^{(n)} - c_1^{(n)}\right) \cdot \sin(\delta) + \left(Q_3^{(n)} - c_3^{(n)}\right) \cdot \cos(\delta)\right]^2}{a_{\text{M}}^{(n)2}} + \frac{Q_2^{(n)2}}{a_{\text{i}}^{(n)2}}$$

$$+ \frac{\left[\left(Q_1^{(n)} - c_1^{(n)}\right) \cos(\delta) - \left(Q_3^{(n)} - c_3^{(n)}\right) \cdot \sin(\delta)\right]^2}{a_{\text{m}}^{(n)2}} - 1 = 0 \tag{2}$$

FIGURE 2 Initial configuration of the plastic domain of the macroelement for the reference soil–abutment system: traces of the yield surfaces (A) in the Q_1–Q_3 and (B) Q_2–Q_3 force spaces

whose centre $c_i^{(n)} = \{c_1^{(n)}, 0, c_3^{(n)}\}$ and semi-axes $a_M^{(n)}, a_i^{(n)}$ and $a_m^{(n)}$ (major, intermediate, and minor semi-axis, respectively) increase linearly from the first yield to the ultimate locus. The yield surfaces evolve during the plastic phase according to a prescribed kinematic hardening rule (see Section 2.6).

2.3 | Inertial effects

Under dynamic conditions, an abutment exhibits a marked frequency-dependent response: the abutment displacements magnify in correspondence of the dominant periods of the soil–abutment system, due to the inertial effects developing in the surrounding soil, causing the transmission of relevant forces to the bridge superstructure.[1,3,5,16]

In the proposed macroelement approach, these inertial effects are simulated by combining the SAME with additional masses, m_i, representing the participating masses of the soil–abutment system for each loading direction. In a dynamic analysis, these masses interact with the activated plastic flows. As the tangent stiffness of the macroelement reduces the natural periods of the system elongate as an effect of the nonlinear soil behaviour.

2.4 | Thermodynamic framework

Although there is an extensive literature available concerning thermodynamic-based formulations for dissipative materials at the meso-scale, the application of this theory to reproduce the behaviour at the macro-scale is currently very limited. To the authors knowledge, apart from the uniaxial macroelement recently developed by Gorini et al.,[1] the only other example is the formulation presented by Le Pape and Sieffert,[17] to simulate the response of shallow foundations under multiaxial loading.

Using the thermodynamic approach, the load-deformation response of the macroelement is fully defined from energy and dissipation potential functions. The energy function can be conveniently expressed in terms of the Gibbs free energy, g, or the Helmholtz free energy, f. These interchangeable state quantities are related by the Legendre transformation, such that $g + f = Q_i \times q_i$.

Because of the marked nonlinear behaviour of soil, the abutment response depends on the entire force–deformation path. This history effect is taken into account in the formulation by the plastic deformations $q_i^{(n)}$ ($n = 1, \ldots, N$) produced in each plastic flow, playing the role of internal variables, such that the total displacement q_i in the i-direction reads:

$$q_i = q_i^{(0)} + \sum_{n=1}^{N} q_i^{(n)} \tag{3}$$

in which $q_i^{(0)}$ is the elastic displacement.

2.4.1 | Energy function

The energy function expresses the work done by the forces acting in the system. More specifically, the Gibbs free energy represents the complementary energy transfer and is described by the following equation:

$$g\left(Q_i^{(1)}, q_i^{(n)}\right) = -W^{(0)} - \sum_{n=1}^{N} W^{(K,n)} + \sum_{n=1}^{N} W^{(H,n)} \tag{4}$$

The term $W^{(0)}$ is the elastic work, while $W^{(K,n)}$ is the so-called *plastic work*, associated with the nth plastic flow, done by the dissipative force $\chi_i^{(n)}$ in the corresponding plastic displacement $q_i^{(n)}$. The *kinematic hardening* work provides energy storage, $W^{(H,n)} > 0$, and is produced during the translation of the nth yield surface; it is controlled by the relative second-order kinematic tensor $H_{ij}^{(n)}$. Accordingly, the Gibbs free energy can be developed as follows:

$$g\left(Q_i^{(1)}, q_i^{(n)}\right) = -\frac{1}{2} \cdot C_{ij}^{(0)} \cdot Q_j^{(0)} \cdot Q_i^{(0)} - \sum_{n=1}^{N} Q_i^{(n)} \cdot q_i^{(n)} + \frac{1}{2} \cdot \sum_{n=1}^{N} H_{ij}^{(n)} \cdot q_j^{(n)} \cdot q_i^{(n)} \tag{5}$$

where $C_{ij}^{(0)}$ is the elastic compliance matrix ($C_{ij}^{(0)} = H_{ij}^{(0)-1}$, with $H_{ij}^{(0)}$ the elastic stiffness matrix) and $q_i^{(k)}$ represents, when $k = 0$, the elastic displacement in the i-direction and the kth plastic displacement when $k = 1,2,\ldots, N$.

Energy transfer can be equivalently expressed by the Helmholtz free energy. By using the Legendre transform, after some manipulation the Helmholtz function assumes the following form:

$$f\left(q_i, q_i^{(n)}\right) = g\left(Q_i^{(1)}, q_i^{(n)}\right) + Q_i^{(1)} \cdot q_i^{(1)} = \frac{1}{2} \cdot H_{ij}^{(0)} \cdot \left(q_j - \sum_{n=1}^{N} q_j^{(n)}\right) \cdot \left(q_i - \sum_{n=1}^{N} q_i^{(n)}\right) + \frac{1}{2} \cdot \sum_{n=1}^{N} H_{ij}^{(n)} \cdot q_j^{(n)} \cdot q_i^{(n)} \tag{6}$$

2.4.2 | Dissipative response

The dissipation potential function d represents the plastic power of the system:

$$d\left(\chi_i^{(n)}, \dot{q}_i^{(n)}\right) = \sum_{n=1}^{N} \chi_i^{(n)} \cdot \dot{q}_i^{(n)} \geq 0 \tag{7}$$

in which $\chi_i^{(n)} = \partial d / \partial \dot{q}_i^{(n)}$ is the dissipative force vector of the nth yield surface that coincides with the nth generalised force vector $\bar{\chi}_i^{(n)} = \partial g / \partial q_i^{(n)}$ for the validity of the orthogonality principle.[15] It can be demonstrated that the true forces $Q_i^{(n)}$ are related to the dissipative forces by the following expression:

$$Q_i^{(n)} = \chi_i^{(n)} + c_i^{(n)}, \quad n = 1, 2, \ldots, N \tag{8}$$

where $c_i^{(n)}$ (centre of the nth yield surface) represents the so-called *back force* due to kinematic hardening (see Section 2.6). To account for the difference between true and dissipative forces produced by hardening, in the thermodynamic formulation the yield surfaces must be expressed as a function of the latter forces, that is, using $\chi_i^{(n)}$ instead of $Q_i^{(n)}$ in Equation (2).

Assuming that the plastic flows are associative, dissipation is directly controlled by the shape of the yield surfaces, $y^{(n)}$, expressed in the space of the dissipative forces $\chi_i^{(n)}$. In fact, the dissipation function, d, can be derived by the following form of the Legendre transform:

$$\lambda^{(n)} \cdot y^{(n)} = \chi_i^{(n)} \cdot \dot{q}_i^{(n)} - d = 0 \tag{9}$$

which can be conveniently rearranged as:

$$d\left(\chi_i^{(n)}, \dot{q}_i^{(n)}\right) = \lambda^{(n)} \cdot \left(\chi_i^{(n)} \cdot \frac{\partial y^{(n)}}{\partial \chi_i^{(n)}} - y^{(n)}\right) \tag{10}$$

in which $\lambda^{(n)} \geq 0$ is the nth plastic multiplier derived according to the following developments.

2.5 | Incremental response

Because of the nonlinear force–displacement relationship of the macroelement, the response needs to be expressed in an incremental form. In this regard, two possibilities exist with respect to each yield surface: the point representing the current equilibrium state is within the nth yield surface ($y^{(n)} < 0$), so it does not contribute to the hardening response, or it lies on the nth yield surface ($y^{(n)} = 0$), then plastic deformations occur during plastic loading as a function of the respective plastic multiplier. In the latter case, the nth yield surface translates with the current internal force so that $\dot{y}^{(n)} = 0$ (consistency condition).

The relationship between the rates of the external forces and the rates of the total displacements can be obtained by differentiating the Helmholtz free energy as follows:

$$\dot{Q}_i = \frac{\partial}{\partial t} \left[\frac{\partial f\left(q_i, q_i^{(n)}\right)}{\partial q_i}\right] = H_{ij}^{(0)} \cdot \left(\dot{q}_j - \sum_{n=1}^{N} \dot{q}_j^{(n)}\right) \tag{11}$$

whose solution requires the definition of the flow rule, associated by hypothesis, for each yield function:

$$\dot{q}_i^{(n)} = \lambda^{(n)} \cdot \frac{\partial y^{(n)}}{\partial \chi_i^{(n)}}, \ n = 1, 2, \ldots, N \tag{12}$$

in which the gradient of the nth yield surface is developed below:

$$\frac{\partial y^{(n)}\left(\chi_i^{(n)}\right)}{\partial \chi_1^{(n)}} = \frac{2 \cdot \sin(\delta)}{a_M^{(n)2}} \cdot \left[\left(\chi_1^{(n)} - c_1^{(n)}\right) \cdot \sin(\delta) + \left(\chi_3^{(n)} - c_3^{(n)}\right) \cdot \cos(\delta)\right]$$

$$+ \frac{2 \cdot \cos(\delta)}{a_m^{(n)2}} \cdot \left[\left(\chi_1^{(n)} - c_1^{(n)}\right) \cdot \cos(\delta) - \left(\chi_3^{(n)} - c_3^{(n)}\right) \cdot \sin(\delta)\right], n = 1, 2, \cdots, N \tag{13}$$

$$\frac{\partial y^{(n)}\left(_i^{(n)}\right)}{\partial \chi_2^{(n)}} = \frac{2 \cdot \chi_2^{(n)}}{a_i^{(n)2}}, n = 1, 2, \cdots, N \tag{14}$$

$$\frac{\partial y^{(n)}\left(\chi_i^{(n)}\right)}{\partial \chi_3^{(n)}} = \frac{2 \cdot \cos(\delta)}{a_M^{(n)2}} \cdot \left[\left(\chi_1^{(n)} - c_1^{(n)}\right) \cdot \sin(\delta) + \left(\chi_3^{(n)} - c_3^{(n)}\right) \cdot \cos(\delta)\right]$$

$$- \frac{2 \cdot \sin(\delta)}{a_m^{(n)2}} \cdot \left[\left(\chi_1^{(n)} - c_1^{(n)}\right) \cdot \cos(\delta) - \left(\chi_3^{(n)} - c_3^{(n)}\right) \cdot \sin(\delta)\right], n = 1, 2, \cdots, N \tag{15}$$

The nth plastic multiplier is determined by invoking the consistency condition $\dot{y}^{(n)} = 0$ and, after some manipulation, it can be written as a function of the nth yield surface and the Gibbs free energy,[18] such as:

$$\lambda^{(n)} = \frac{\partial y^{(n)}\left(\chi_i^{(n)}\right)/\partial \chi_i^{(n)} \cdot \dot{Q}_i^{(n)}}{\partial y^{(n)}\left(\chi_i^{(n)}\right)/\partial \chi_i^{(n)} \cdot \partial^2 g_2\left(q_i^{(n)}\right)/\partial q_i^{(n)} \partial q_j^{(n)} \cdot \partial y^{(n)}\left(\chi_i^{(n)}\right)/\partial \chi_j^{(n)} - \partial y^{(n)}\left(\chi_i^{(n)}\right)/\partial q_i^{(n)} \cdot \partial y^{(n)}\left(\chi_i^{(n)}\right)/\partial \chi_i^{(n)}}$$

$$= \frac{\partial y^{(n)}\left(\chi_i^{(n)}\right)/\partial \chi_i^{(n)} \cdot \dot{Q}_i^{(n)}}{\partial y^{(n)}\left(\chi_i^{(n)}\right)/\partial \chi_i^{(n)} \cdot \partial^2 g_2\left(q_i^{(n)}\right)/\partial q_i^{(n)} \partial q_j^{(n)} \cdot \partial y^{(n)}\left(\chi_j^{(n)}\right)/\partial \chi_j^{(n)}}, \quad n = 1, 2, \dots, N \qquad (16)$$

in which the term $\partial y^{(n)}(\chi_i^{(n)})/\partial q_i^{(n)} = 0$ because the yield functions do not depend on the plastic displacements. In other words, during plastic loading the nth yield surface translates in the true force space but its shape and size remain unaltered (kinematic hardening), implying that it does not evolve in the space of the dissipative forces $\chi_i^{(n)}$.

The second derivative with respect to the plastic displacements of the sub-function $g_2\left(q_i^{(n)}\right) = 1/2 \cdot \sum_{n=1}^{N} H_{ij}^{(n)} \cdot q_j^{(n)} \cdot q_i^{(n)}$, that is the part of the Gibbs free energy depending only on the internal variables, is exactly equal to $H_{ij}^{(n)}$, so that the nth plastic modulus reads:

$$H_{\text{pl}}^{(n)} = \frac{\partial y^{(n)}\left(\chi_i^{(n)}\right)}{\partial \chi_i^{(n)}} \cdot H_{ij}^{(n)} \cdot \frac{\partial y^{(n)}\left(\chi_j^{(n)}\right)}{\partial \chi_j^{(n)}}, \quad n = 1, 2, \dots, N \qquad (17)$$

2.6 | Kinematic hardening

When the force state lies on the nth yield surface, plastic deformations occur when $\lambda^{(n)} > 0$ (plastic loading). The kinematic hardening of the nth yield surface is provided by the translation rule for the centre of the surface in the force space, which, for thermodynamic consistency, derives from the energy function as described below.

By virtue of the lack of coupling of the elastic–plastic response assumed in the present formulation, the Gibbs free energy can also be regarded as the sum of three separate terms[14]:

$$g\left(Q_i^{(1)}, q_i^{(n)}\right) = g_1\left(Q_i^{(1)}\right) + g_2\left(q_i^{(n)}\right) - \sum_{n=1}^{N} Q_i^{(n)} \cdot q_i^{(n)} \qquad (18)$$

where, in particular, $g_2(q_i^{(n)})$ is a function of the load history through the plastic displacements $q_i^{(n)}$, conferring the desired kinematic hardening response. By introducing Equation (18) into the definition of the generalised force, $\bar{\chi}_i^{(n)}\left(q_i^{(n)}\right) = -\partial g/\partial q_i^{(n)}$, the latter becomes:

$$\overline{\chi}_i^{(n)}\left(q_i^{(n)}\right) = -\frac{\partial}{\partial q_i^{(n)}}\left[g_1\left(Q_i^{(1)}\right) + g_2\left(q_i^{(n)}\right) - \sum_{n=1}^{N} Q_i^{(n)} \cdot q_i^{(n)}\right] = -\frac{\partial}{\partial q_i^{(n)}}\left[g_2\left(q_i^{(n)}\right) - \sum_{n=1}^{N} Q_i^{(n)} \cdot q_i^{(n)}\right]$$

$$= -\frac{\partial g_2\left(q_i^{(n)}\right)}{\partial q_i^{(n)}} + Q_i^{(n)}, \quad n = 1, 2, \dots, N \qquad (19)$$

so that the nth generalised force turns out to be the difference between the true force $Q_i^{(n)}$ and the back force $c_i^{(n)} = \partial g_2(q_i^{(n)})/\partial q_i^{(n)}$. Therefore, the translation rule for the yield surfaces is governed by the time derivative of the
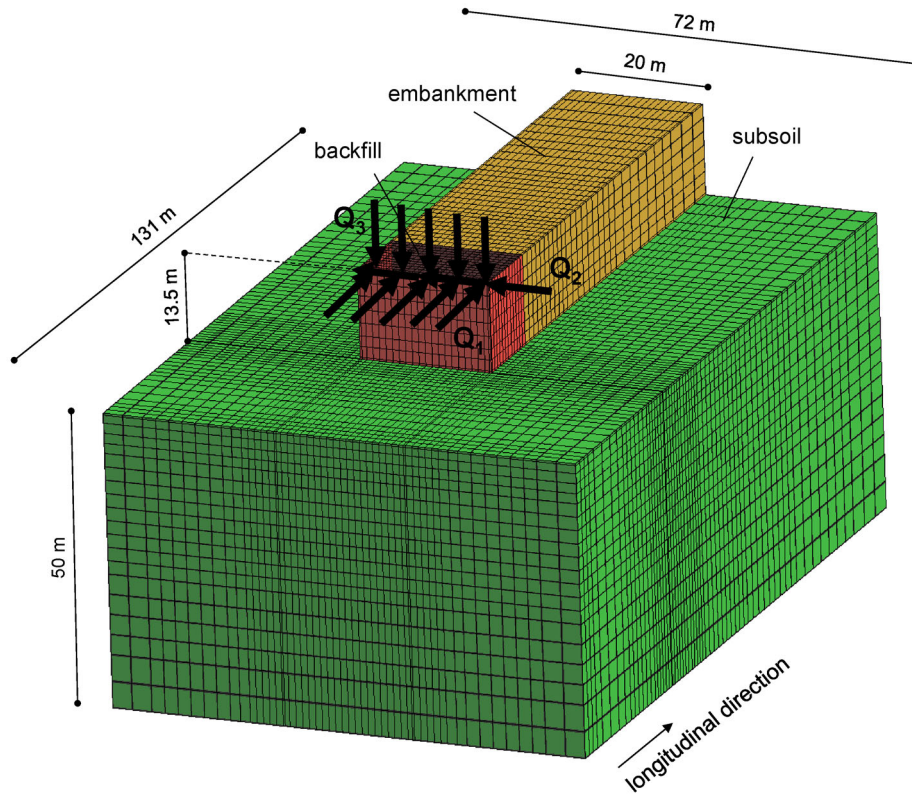
FIGURE 3   Reference soil–abutment interaction model (CC model) implemented in OpenSees

back force as follows:

$$\dot{c}_i^{(n)} = \frac{\partial^2 g_2\left(q_i^{(n)}\right)}{\partial q_i^{(n)2}} \cdot \dot{q}_j^{(n)} = H_{ij}^{(n)} \cdot \dot{q}_j^{(n)}, \ n = 1, 2, \dots, N \tag{20}$$

from which it can be observed that $\dot{c}_i^{(n)}$ is collinear with the plastic displacement increment vector $\dot{q}_j^{(n)}$ only when the kinematic stiffness tensor $H_{ij}^{(n)}$ is diagonal.

3 | CALIBRATION

The calibration of the macroelement requires the definition of (1) the ultimate yield surface, defining the entire plastic domain, (2) the initial stiffness matrix, and (3) the participating masses of the soil–abutment system, m_i. Although different calibration procedures were devised for different abutment typologies, the following discussion is limited to the case of seat-type abutments, for the sake of brevity.

3.1 | Reference case study

Figure 3 shows a numerical soil–abutment model which we consider as a reference to illustrate the salient features included in the macroelement. This model, implemented in the analysis framework OpenSees,[19,20] assume the same sub-soil conditions described in Gorini et al.[3] The abutment is a massive reinforced concrete structure with a 13.5 m-height wall supported by a shallow foundation with length of 9.5 m. The thickness of the front wall and of the foundation is equal to 1.5 m. The uniform soil domain is assumed to be dry and reflects the mechanical properties of the Messina Gravels.[5,11,21,22] The soil mass is discretised through SSPbrick eight-node hexahedral elements[23] with mechanical behaviour described by

TABLE 1   Parameters of the PDMY model adopted for the foundation soil and the embankment in the CC model

Variable	Description	Foundation soil	Embankment
ρ (Mg/m^3)	Mass density	2.243	2.039
G_r (kPa)	Elastic shear modulus at p_r'	1.3×10^5	1.5×10^5
ν	Poisson's ratio	0.2	0.2
p_r' (kPa)	Reference mean pressure	80.0	80.0
D	Pressure dependent coefficient	0.5	0.5
$\gamma_{d,max}$	Peak shear strain	0.1	0.1
φ_{PTL}	Phase transformation angle	26°	26°
C	Contraction parameter	0.195	0.195
d_1	Dilation parameters	0.6	0.6
d_2		3.0	3.0
M	Critical stress ratio	1.54	1.42
λ_c		0.022	0.022
e_0	Critical state line parameter	0.448	0.448
ξ		0.7	0.7
N	Number of yield surfaces	40	40

the PDMY model developed by Yang et al.[24] The latter is formulated within a multi-surface plasticity framework[25] and is aimed at reproducing the cyclic response of coarse-grained soils. The model uses a set of conical yield surfaces with a common apex at zero mean effective stress and that evolve with a deviatoric kinematic hardening. The PDMY provides a pressure-dependent piecewise-linear stress–strain relationship from small strain levels to the ultimate conditions. The small-strain shear modulus G_0 is a function of the mean effective stress p' as $G_0 = G_R(p'/p_R')^d$, where G_R is the small-strain modulus at a reference mean effective stress, p_R', and d is a material constant controlling the evolution of stiffness with the effective stress. The PDMY model is able to reproduce the dependence of energy dissipation of soil on the strain amplitude. Non-associativity of the plastic flow is restricted to its volumetric component according to an empirical flow rule. This assumption causes the model however to overestimate the plastic volumetric strains induced by changes in deviatoric stress.[11,24,26] For the case under examination (Figure 3), the input parameters of the model are reported in Table 1, as the ones determined in a previous study referring to a large number of experimental data.[5,11]

For simplicity, the embankment was modelled with an equivalent, rectangular cross-section, impeding the horizontal relative displacements at the opposite faces. This can be regarded as a reasonable approximation of the actual trapezoidal shape in the evaluation of the seismic actions exchanged between abutment and embankment.[27–30] This technique neglects the occurrence of local instabilities along the embankment slopes during a seismic event, that is likely the case of a reinforced earth body.

In the finite-element model, the soil–structure contact was modelled as thin layers of solid elements interposed between the structure and the soil. The structural members of the abutment were modelled by using the ShellMITC4 elements[31] with visco-elastic behaviour, and adopting constitutive parameters relative to the C32/40 strength class concrete in the European standards, EN 206-1. In order to reproduce the actual stress state in the soil under static conditions, the model was built by using a staged analysis procedure, including a preliminary gravity analysis of the subsoil, followed by the construction of the abutment and the embankment.

The initial state of the macroelement represents the end of construction of the embankment–abutment system. As a standard practice in the case of multi-span girder bridges, it was assumed that the embankment–abutment system is built before the connection of the abutment with the deck. Accordingly, the initial force state in the SAME corresponds to null interaction forces transferred by the deck and the plastic domain takes implicitly into account the level of mobilised strength in the soil at the end of the embankment construction.

3.2 | Identification of the ultimate limit state surface

Under the assumption of homothetic yield surfaces, the shape and orientation of the plastic domain can be derived from those of the ultimate surface. According to Gorini et al.,[6,7] the latter can be fully related to the limit value of the vertical
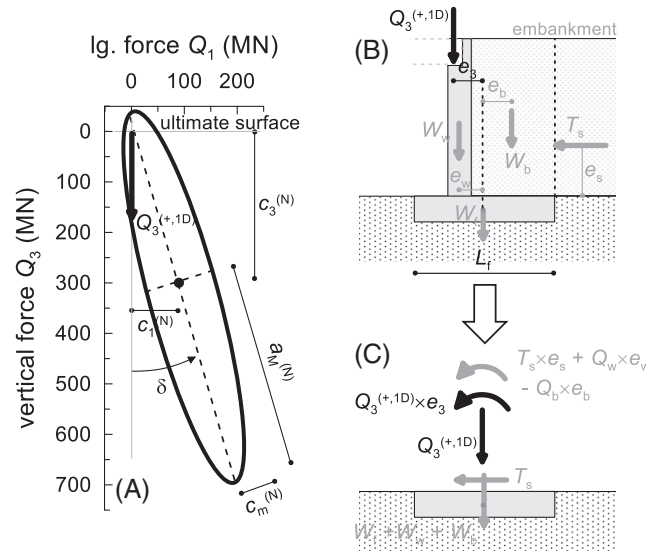
FIGURE 4 (A) Ultimate limit state surface for the reference soil–abutment system and related parameters; (B) effective load pattern associated with the evaluation of the limit downwards force, $Q_3^{(+,1D)}$ and (C) simplified layout for its evaluation

downward force transmitted by the abutment front wall to the foundation, $Q_3^{(+,1D)}$, and by the orientation of the ellipsoid, δ, that varies between 14° and 16° for seat-type abutments. The aspect ratio of the ultimate locus depends primarily on the abutment typology. For seat-type bridge abutments, the shape ratios $a_M^{(N)} / a_m^{(N)}$ and $a_M^{(N)} / a_i^{(N)}$ between the semi-axes of the ultimate ellipsoid (see Figure 4A) can be taken equal to 5.0 and 2.3, respectively, according to the geometry of the abutment under examination.[6] The centre of the locus can be assumed as $c_1^{(N)} = 0.31 \times a_M^{(N)}$ and $c_3^{(N)} = 0.92 \times a_M^{(N)}$.

The limit force $Q_3^{(+,1D)}$ is the vertical force transferred by the bridge deck to the abutment that produces its collapse under the load combination depicted in Figure 4B,C. In addition to the vertical force transferred by the deck, the loading combination includes the self-weight of the abutment and of the soil fill resting on the footing, W_i, and the soil thrust, T_s, resulting in an inclined load and a moment acting on the foundation. Under these conditions, $Q_3^{(+,1D)}$ can be calculated through the conventional approaches used for shallow and deep foundations loaded by eccentric and inclined loads (for piled foundations, Gorini and Callisto[32] developed a numerical tool that allows for a prompt evaluation of $Q_3^{(+,1D)}$). The resulting ultimate locus in the Q_1-Q_3 space for the reference soil–abutment system (Section 3.1) is illustrated in Figure 4A.

The number of yield surfaces composing the macroelement controls the smoothness of the piecewise linear force–displacement relationship. In the present study, five yield surfaces were deemed sufficient, but it should be noted that the number of surfaces has a minor influence on the computational effort, as it increases only the iterations in the material sub-routine but does not alter the number of degrees of freedom of the model.

3.3 | Initial stiffness and modal characteristics of the soil–abutment system

The initial stiffness of the macroelement is controlled by the tensor $H_{ij}^{(0)}$, describing the stiffness in the elastic region, that has to be related to additional masses, acting on the translational degrees of freedom of the deck–abutment contact, to reproduce the desired frequency-dependent response at small strain levels. For the sake of simplicity, the stiffness tensors $H_{ij}^{(n)}$ ($n = 0,1,\ldots,N$) were assumed to be diagonal, hence the directional coupling of the macroelement response is only produced by the development of plastic displacements (associated flow rule). Previous works showed that, for each coordinate direction of the deck–abutment contact, a soil–abutment system with shallow foundation exhibits a marked mono-modal response, evolving with the level of mobilised strength in the soil.[1,3] It was therein demonstrated that this feature can be efficiently simulated including in the uniaxial version of the macroelement the mass that participates to the vibration of the soil–abutment system at small strains, that is, when the soil deforms elastically. This procedure, previously delineated under uniaxial conditions,[1] can be generalised to multiaxial loading as follows. The masses and vibration periods, m_i and $T_i^{(0)}$, $i = 1,2,3$, of the geotechnical system in the linear regime can be obtained by using available analytical solutions.[3] It may be assumed that the elongation of the natural vibration periods produced by the soil nonlinearity

TABLE 2 Masses, m_i, and small-strain stiffness tensor, $H_{ij}^{(0)}$, of the macroelement for the reference case study

| Direction	m_i (Gg)	$m_i / (m_S + m_B)$	$H_{ij}^{(0)}$ (GN/m)
Long. - 1	35.9	6.4	12.8
Transv. - 2	23.9	4.3	4.3
Vert. - 3	42.1	7.5	39.5
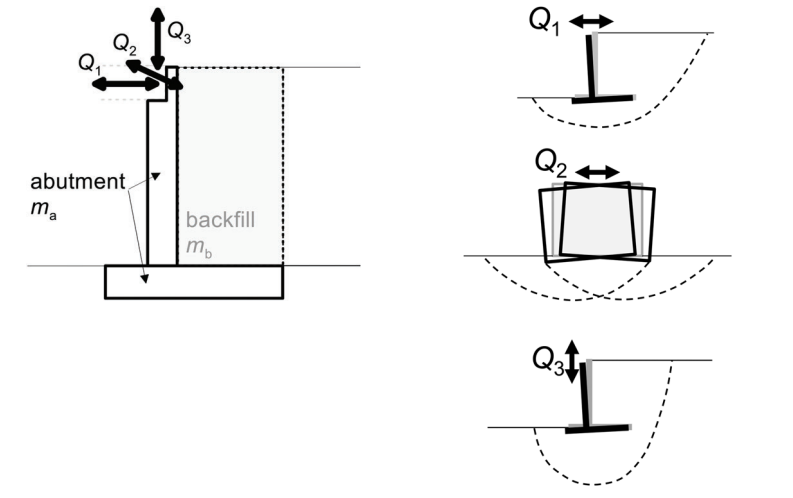
starts when the mobilised strength $Q_i/Q_i^{(max)}$ exceeds about 30%.[1,3] To reproduce this effect, the stiffness tensor $H_{ij}^{(1)}$, controlling the kinematic hardening of the first yield surface, is assumed equal to $H_{ij}^{(0)}$. The equivalent stiffness of the macroelement when the first plastic flow is activated is therefore equal to $H_{ij}^{(eq)} = 0.5H_{ij}^{(0)}$ and can be obtained by the equation of the vibration period of a single degree of freedom system. For the reference case study, the resulting small-strain vibration periods of the soil–abutment system are equal to 0.47, 0.67, and 0.29 s in the longitudinal, transverse, and vertical directions, respectively; the corresponding small-strain mass and stiffness tensors of the macroelement are listed in Table 2.

The higher order stiffness tensors, $H_{ij}^{(n>1)}$, are derived assuming a hyperbolic variation of the tangent stiffness from small strains to failure, as a multiaxial generalisation of the evolution law proposed by Gorini et al.[1] for the one-dimensional macroelement.

4 | USE IN STRUCTURAL ANALYSIS AND IMPLEMENTATION

In the use of the macroelement to reproduce soil-structure interaction, two idealised soil regions are considered: (i) the near field, intended as the soil zone that interacts directly with the structure, and (ii) the far field, which is not influenced by the presence of the structure. The macroelement is called upon to simulate the behaviour of the near-field soil region, while the propagation of the seismic waves from the bedrock up to the boundary of the near field is studied through a free-field ground response analysis. The seismic motion computed at the boundary of the near field is then used as an input for the macroelement in the global structural model. For an abutment with a shallow foundation the near-field soil region should be extended to an effective depth z_{eff} equal to the width L_f of the abutment in the longitudinal direction[1] (L_f shown in Figure 4B). For an abutment on piled foundation, the effective depth is the maximum of either L_f or $10d_p$[7] (where d_p is the pile diameter).

The proposed macroelement (SAME) was implemented in OpenSees, an object-oriented framework for finite element analysis.[19,20] The implementation consisted in the definition of a new *NDMaterial* subclass, that is a multiaxial constitutive relationship coded using the C++ programming language. This constitutive law can be assigned to a multiaxial zero-length finite element, *ZeroLengthND*, available in the OpenSees library, that establishes an explicit nonlinear relationship between two overlapped nodes. The frequency-dependent effects are reproduced by assigning the masses m_i directly to the node where the deck is constrained to the abutment in the global structural model.
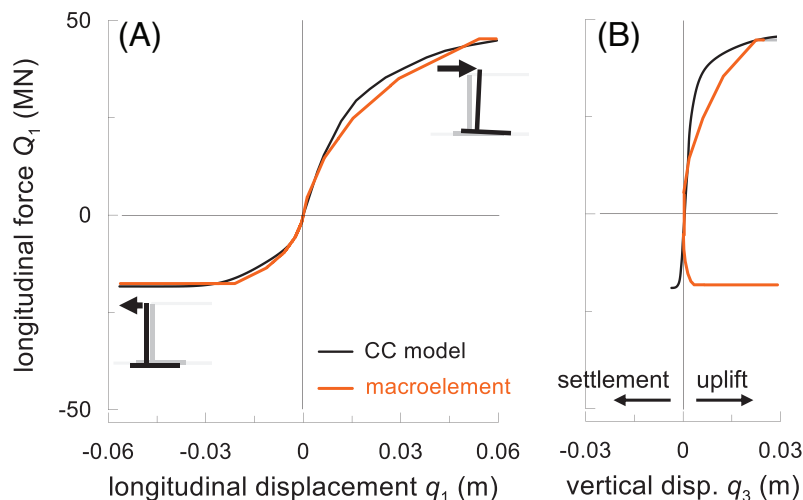
FIGURE 5 Comparison between the responses of the CC model and of the macroelement under monotonic longitudinal loading: (A) Q_1-q_1 curves and (B) effect of the directional coupling of the plastic response

The macroelement can simulate the response of the soil–abutment system under both static and dynamic conditions. The SAME assumes a fully drained behaviour for the embankment, typically made up of partially saturated sandy soil with high permeability, whilst a fully drained or undrained behaviour (total stress conditions) of the foundation soil, depending on the soil category and on the analysis type (static or transient). In the static stages, for example, representing the construction sequence of the bridge, the end node of the macroelement (boundary of the near field) is fully restrained. In the subsequent dynamic analysis, these restraints are removed and the seismic motion, consisting of ground motion time histories deriving from a free-field site response analysis, is applied to the end node.
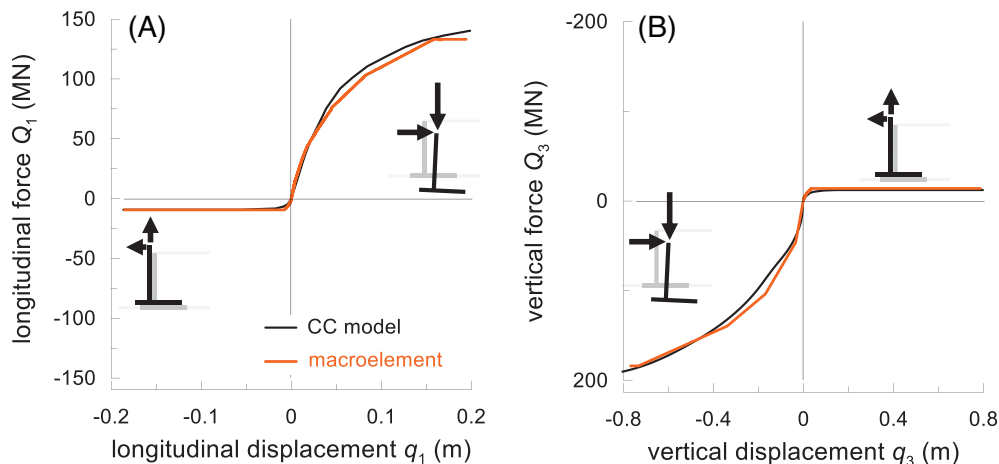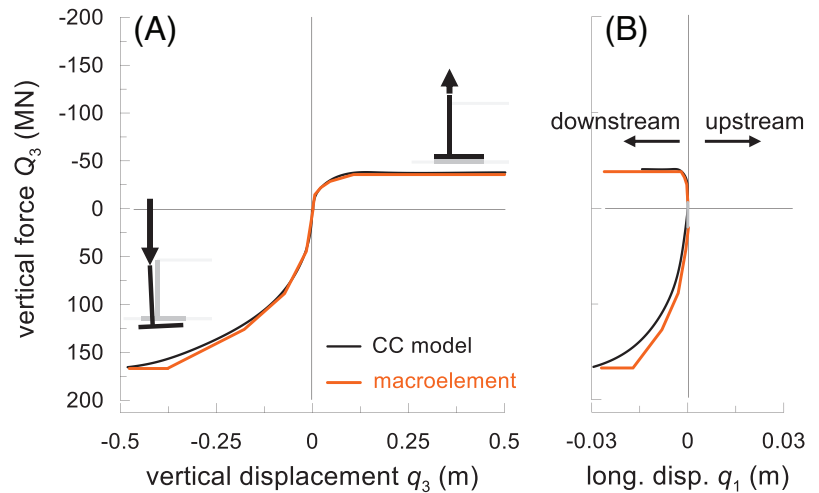
5 | MONOTONIC RESPONSE

The response of the macroelement (calibrated as described in Section 3), was tested considering numerous load paths, under monotonic and dynamic conditions. The continuum coupled (CC) soil–abutment model in Figure 3 was considered as an advanced reference for comparison. Under monotonic loading conditions, a series of force-controlled pushover analyses were carried out using the proposed macroelement (SAME) and the CC model, comparing the hardening response from small to large strain levels. To simulate the actions transmitted by the deck, in the coupled model progressively increasing forces were applied to the top nodes of the front wall, monitoring the resulting displacement. The boundaries of the subsoil domain maintain the conditions imposed during the static stages (see Section 3.1). Using SAME, these load conditions are reproduced by simply applying the external force to one node, keeping the other one fixed.

5.1 | Uniaxial perturbation

Figure 5 compares the response of the two models perturbed by a purely longitudinal force, Q_1. The resulting q_1-Q_1 relationships are in a good agreement and show the strong asymmetry in the longitudinal response of the abutment. In spite of the limited number of yield surfaces used in the present case, equal to 5, SAME captures quite well the evolution of the tangent longitudinal stiffness of the coupled soil–abutment system, validating the hyperbolic variation of the stiffness tensors associated with the plastic flows of SAME. The force Q_1 produces also a vertical displacement of the abutment top (Figure 5B). The uplift of the abutment under passive limit conditions obtained in the coupled model is well reproduced by the macroelement. However, the associated flow rule used in the macroelement formulation produces an uplift of the abutment also for active limit conditions. This effect, disproved both by the results of the coupled model and by common experience, is due to the local slope of the yield surfaces at zero vertical force (see for instance Figure 4A). In any practical use of the macroelement, this minor inaccuracy (the vertical displacement occurring before the attainment of the ultimate capacity is very small, about 2 mm) is neutralised by the presence of the vertical load transmitted by the bridge deck, that readily reverses the local slope of the yield surfaces.

FIGURE 6 Comparison between the responses of the CC model and of the macroelement under monotonic vertical loading: (A) Q_3-q_3 curves and (B) effect of the directional coupling of the plastic response
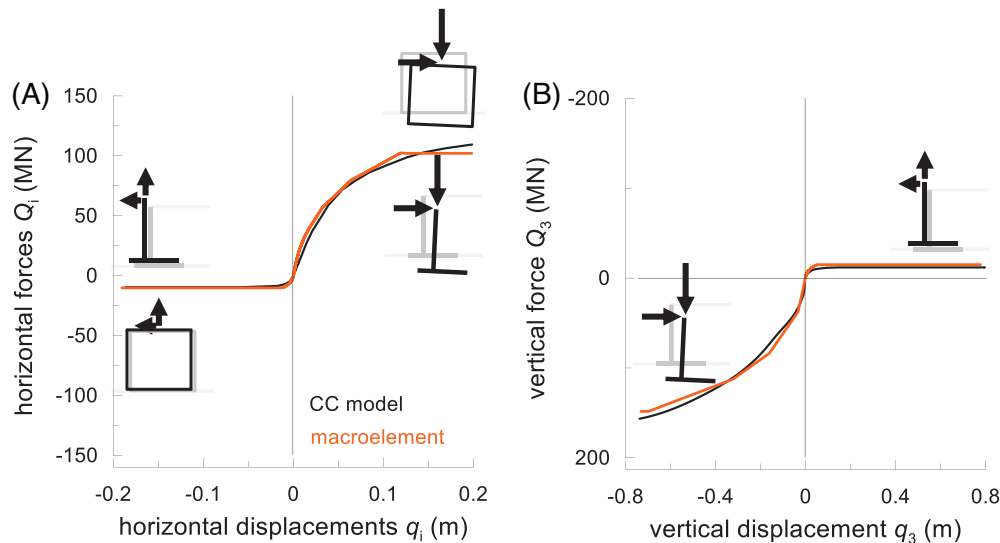

FIGURE 7 Comparison between the responses of the CC model and of the macroelement under monotonic longitudinal-vertical loading: (A) Q_1-q_1 and (B) Q_3-q_3 relationships

The application of a vertical force, Q_3, produces more substantial asymmetry in the abutment response. This is shown in Figure 6A, where it can be seen that the uplift mechanism is much weaker than the downward limit mechanism. The proposed macroelement SAME is able to capture satisfactorily these aspects of the vertical response, as well as the effects of the directional coupling in the nonlinear regime: Figure 6B shows that as a consequence of a vertical displacement the abutment moves away from the embankment, and this is well simulated by the flow rule in SAME.

5.2 | Multiaxial response

The simultaneous application of the two loads Q_1 and Q_3 leads to the response shown in Figure 7, for a load ratio $Q_3/Q_1 = 1.5$. The SAME model reproduces quite closely the multiaxial response of the advanced model. The main discrepancies are observed at large strains, when the passive resistance of the soil is mobilized ($Q_1 > 0$ and $Q_3 > 0$). Under these conditions, SAME provides a constant limit force when the ultimate limit state surface is reached, while in the CC model the tangent stiffness of the q_1-Q_1 curve at large strain levels is approximately equal to 10% the initial one. This hardening response at the macro-scale may be due to the integration of the constitutive response of the PDMY used in the CC model, presenting a small hardening at failure to facilitate numerical stability, on a large number of soil elements, producing a stress redistribution in the subsoil even for very large external forces (inclined asymptote of the q_1-Q_1 curve at large strain levels).

FIGURE 8 Comparison between the responses of the CC model and of the macroelement under monotonic longitudinal-transverse-vertical loading: (A) horizontal and (B) Q_3-q_3 relationships

Figure 8 illustrates the response of the macroelement when a transverse force $Q_2/Q_1 = 1.0$ is applied while maintaining a ratio of the vertical to the longitudinal forces $Q_3/Q_1 = 1.5$. The presence of a transverse force reduces the limit values of the longitudinal and vertical forces (compare Figures 7 and 8) activating a combined plastic mechanism. Despite the symmetry of the system with respect to the longitudinal plane, the transverse response is highly non-symmetric due to the multi-axiality of the force state, which calls into play the asymmetric responses shown in directions 1 and 3. Figure 8 shows that the proposed macroelement is able to simulate very well this complex multiaxial behaviour along the entire loading path.

6 | DYNAMIC RESPONSE

6.1 | Validation procedure

While the uniaxial cyclic response of the macroelement was validated in a previous work,[1] in this study the focus is on the response of the 3D macroelement, SAME, that is compared with the behaviour of the continuum coupled (CC) soil–abutment model. The validation is based on the conceptual scheme illustrated in Figure 9. A preliminary structural analysis of a bridge model with fixed constraints was carried out, to determine realistic seismic actions exchanged at the abutment–deck contact that were then used to load the macroelement and the coupled soil–abutment system.

Four seismic records (Kobe, Tabas, Kocaeli and Iwate) were considered as representative of the seismicity on a stiff outcrop for the site at hand.[5] The corresponding elastic response spectra of the longitudinal motion are shown in Figure 9 together with the design spectrum relative to a severe earthquake scenario. The three-component seismic records were propagated through the foundation soils by carrying out a free field site response analysis, obtaining the seismic motion at the effective depth $z_f = L_f = 9.5$ m (see Section 4). The propagated motion represented the seismic excitation for the global structural model of the bridge, on which nonlinear dynamic analyses with fixed constraints were carried out, considering the three-component motion applied to all supports (stage 2 in Figure 9). In the coupled model, the nodal reactions calculated at the strong abutment (i.e., the one longitudinally connected to the deck) in the directions 1, 2 and 3 were applied to the top of the front wall, while the same forces were applied to the free node of the proposed SAME, performing dynamic analyses in the time domain for both the CC model and SAME. To model the inertial response of the macroelement, the masses m_i determined in Section 3 were attached to the free node along each loading direction.

In order to illustrate the computational efficiency of the macroelement, Table 3 reports the calculation times needed for the SAME and CC model using both the standard OpenSees solver and the parallel solver based on domain decomposition, OpenSeesSP.[33] The computation times refer to a multi-core workstation with 16 dual-core central processing units (overclocked to 3.7 GHz with a 60 Gbytes RAM). The results highlight excessive/impractical computation times for the
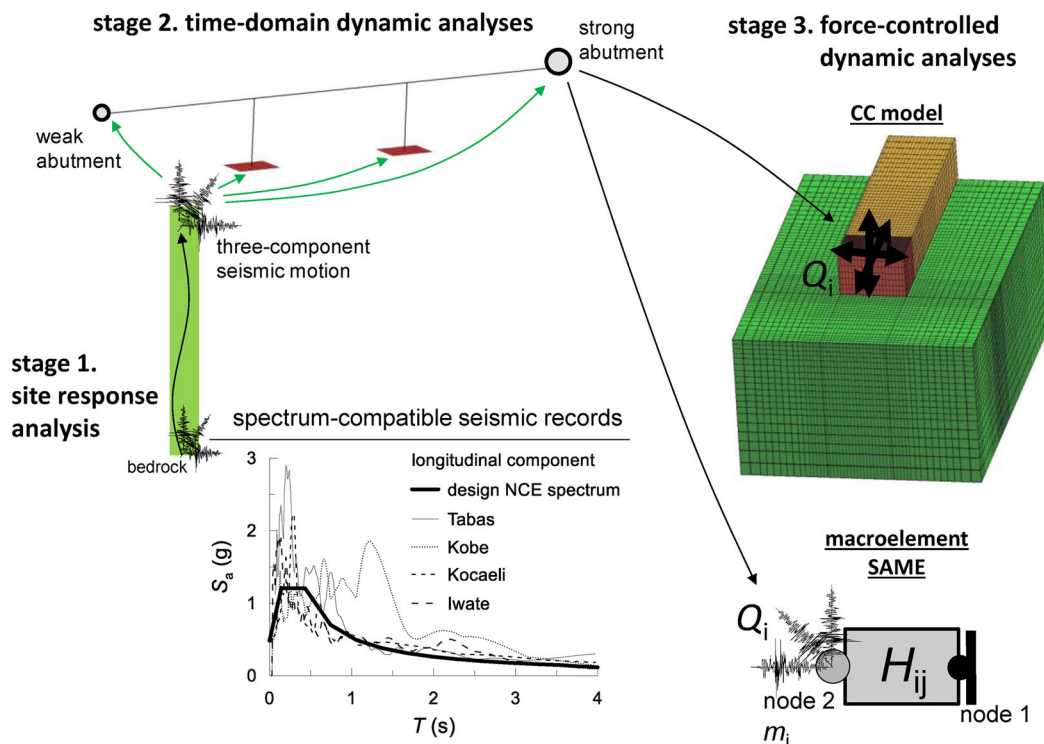
FIGURE 9   Validation procedure of the macroelement

TABLE 3   Computation times of the nonlinear dynamic analyses with three-component force time histories on the CC model, using sequential and parallel computing, and on the macroelement

Seismic scenario	CC model		Macroelement
	OpenSees	OpenSeesSP	
Kobe	48 days	7.1 days	5 min
Tabas	51 days	7.5 days	6 min
Kocaeli	45 days	6.7 days	4 min
Iwate	54 days	8.1 days	6 min

CC model (averaging 7.4 days even for the efficient parallel solver, OpenSeesSP), while analyses with the proposed SAME model were accomplished ~5 min.

In the following, we analyse in detail the comparison between the global response of the abutment using the continuum coupled (CC) model and the proposed macroelement (SAME) using the loading history obtained for the Kobe record, Figure 10. Similar results for the three other earthquake records are reported in Appendix.

6.2 | Uniaxial seismic response

Figure 11 shows the comparison between the responses of the SAME and CC models perturbed by the longitudinal external force of the Kobe record (Figure 10A) (note that the static vertical force is always present). The results are expressed in terms of the longitudinal displacement, q_1, of the top of the front wall and of the external force, Q_1.

The seismic performance of the abutment is well reproduced by the inertial macroelement. The time evolution of the displacement of the abutment top (Figure 11A) shows a clear asymmetry in the response, with the accumulation of a significant permanent displacement away from the embankment ($q_1 < 0$) in the interval of maximum intensity of Q_1, between 9 and 15 s. This is a typical feature in the dynamic response of bridge abutments, and it has also been observed in related studies aimed at evaluating the influence of the mass participation of the soil interacting with the abutment.[1,3,5] The resulting force–displacement relationship of the macroelement (Figure 11B) is similar to that obtained with the coupled model, albeit with slightly more closed cycles.
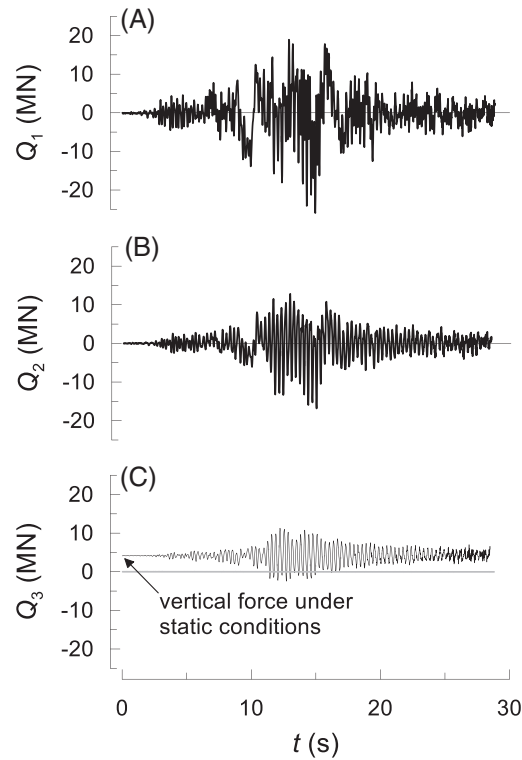
FIGURE 10   Time-histories of the (A) longitudinal, (B) transverse and (C) vertical forces at the deck–abutment contact obtained with the structural analysis with fixed base subjected to the Kobe earthquake
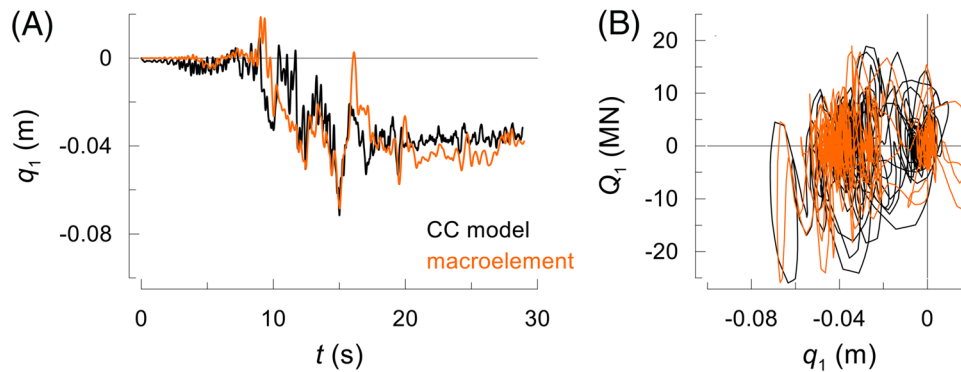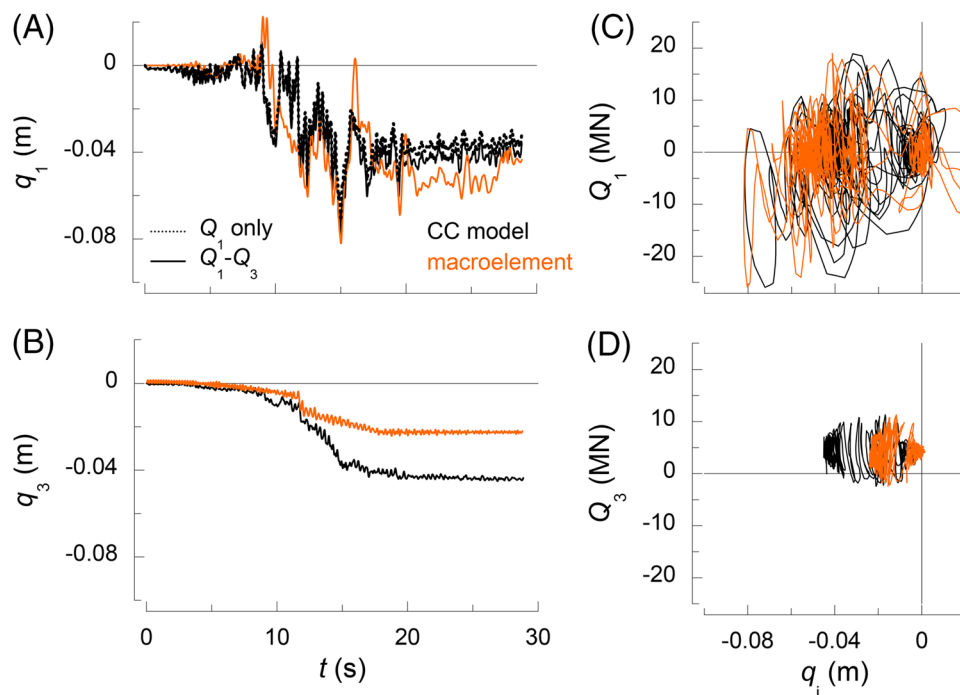

FIGURE 11   Comparison between the responses of the CC model and of the macroelement perturbed by the longitudinal force time history relative to the Kobe earthquake: (A) time evolution of the displacement q1 and (B) Q_1-q_1 relationship

6.3 | Effect of the multi-directionality of the seismic action

Keeping the focus on the response in the longitudinal–vertical plane of the abutment, Figure 12 shows the abutment response obtained by perturbing the coupled model and the macroelement with the time histories of the longitudinal and vertical forces, Q_1 and Q_3, of the Kobe record. In the longitudinal direction, SAME reproduces quite satisfactorily the response of the CC model (Figure 12A), in terms of both the maximum amplitudes and the accumulation of permanent displacements of the abutment.

The simultaneous presence of Q_1 and Q_3 increases slightly the displacements in the longitudinal direction compared to the case without vertical component (dashed line in Figure 12A). This moderate effect is due to the low intensity of the external vertical force components compared with those in the longitudinal direction. The temporal evolution of the displacements (Figure 12B) shows that the vertical action does not excite significantly the soil–abutment system, with
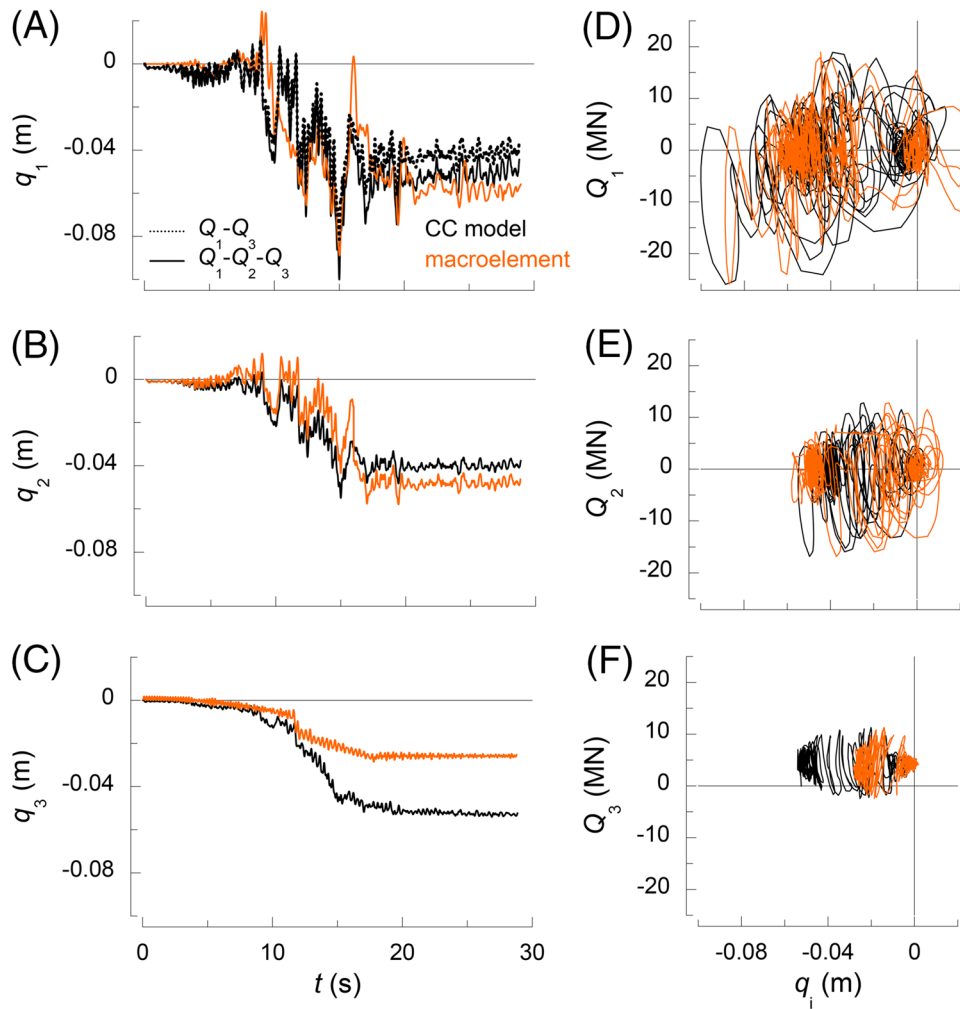
FIGURE 12 Comparison between the responses of the CC model and of the macroelement perturbed by the longitudinal-vertical force time-histories relative to the Kobe earthquake: (A–B) time evolution of the displacements q_1 and q_3, and (C–D) Q_1-q_1 and Q_3-q_3 relationships

oscillations visibly characterized by higher frequencies than those associated with the longitudinal response (the small-strain vibration periods of the soil–abutment system in the longitudinal and vertical directions are equal to 0.47 and 0.29 s, respectively). However, the vertical component of the dynamic load leads to significant permanent settlements at the top of the abutment. As it will appear more evident later on, the marked irreversibility exhibited in the vertical direction derives from the directional coupling of the response. In fact, the progressive shift of the abutment displacement occurs in the interval of maximum intensity of the longitudinal load: the soil strength is mobilized according to a combined deformation mode of the abutment, leading to the development of irreversible displacements in both directions. The magnitude of these irreversible effects depends on the flow rule of the constitutive laws used in the two models, whose main features were discussed in Section 3.1. As a result of a systematic comparison between the PDMY response and experimental data at the soil element scale and examining the dynamic response of fully coupled and reduced-order soil-bridge models,[11,16,26] it was seen that the PDMY soil model tends to overestimate the plastic volumetric strains produced by deviatoric stress component. This is the main reason why the CC model generates significant permanent settlements of the abutment. In contrast, the macroelement produces more limited settlements that derive from its thermodynamic-based associated flow rule. The combination of the effects above can be deemed responsible of the discrepancy in the permanent settlements evidenced in Figure 12. However, there are no experimental studies available that document irreversible abutment deformations induced by seismic loading. For these reasons, it is difficult to assess objectively the accuracy of the two modelling approaches in simulating the permanent settlements induced by horizontal actions.

The distinct features of the abutment response discussed above are also reflected in the dynamic response under three-axis loading conditions, shown in Figure 13. Apart from the discrepancies on the permanent vertical displacements, the instantaneous oscillations in the vertical direction are somewhat comparable, indicating that the vertical dynamic amplification of the system is well reproduced by the proposed SAME (Figure 13C). The latter simulates quite accurately the abutment response predicted by the more comprehensive CC model in the horizontal plane, including the accumulation of transverse displacements q_2. This is a direct result of the coupled model that is reproduced at the macroelement scale through the asymmetry of the plastic domain. For instance, Figure 14 shows the horizontal load path together with the projections of the ultimate yield surface in the planes $Q_3 = 0$ (longitudinal–transverse force space) and $Q_3 = Q_3^{(st)}$ ($Q_3^{(st)}$ is the static vertical force transferred by the deck): these are ellipses with a major axis parallel to the Q_1-axis but translated with respect to the origin (passive resistance larger than the active one). For multiaxial loading, the horizontal limit force is therefore significantly lower when Q_1 is directed away from the embankment, producing a non-symmetrical development

FIGURE 13 Comparison between the responses of the CC model and of the macroelement perturbed by the longitudinal-transverse-vertical force time-histories relative to the Kobe earthquake: (A–B–C) time evolution of the displacements q_1, q_2 and q_3, and (D–E–F) Q_1-q_1, Q_2-q_2 and Q_3-q_3 relationships
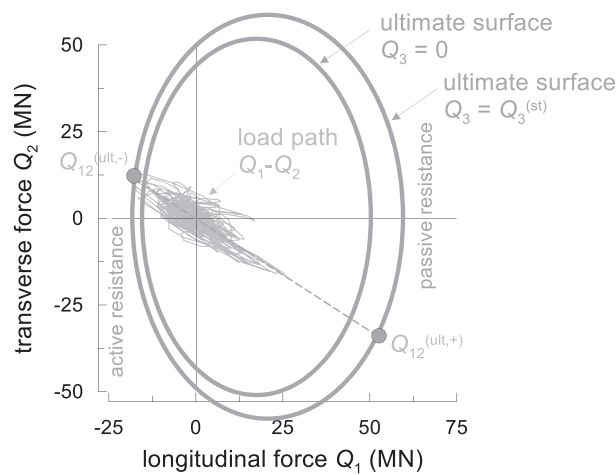
FIGURE 14 Horizontal load path and representation of the traces of the ultimate surface of the macroelement in the plane Q_1-Q_2, for $Q_3 = 0$ and $Q_3 = Q_3(st)$ ($Q_3(st)$ = vertical load under static conditions)
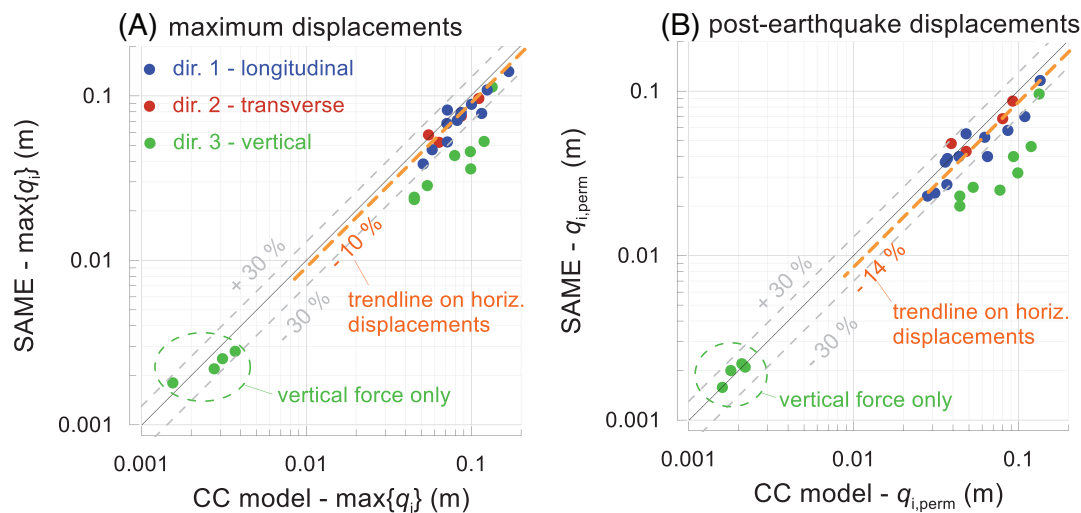
FIGURE 15 (A) Maximum and (B) permanent displacements of the macroelement (SAME) plotted as a function of the relative values computed with the continuum coupled (CC) model, for all seismic scenarios

of irreversible transverse displacements induced by the attainment of the active resistance in the longitudinal direction ($Q_{12}^{(\text{ult},-)}$ in Figure 14).

6.4 | Seismic performance of the abutment: summary of the parametric study

The performance of the reference abutment has been studied with both the CC model and SAME for seismic records of three other earthquakes, Tabas, Kocaeli and Iwate. The results are concisely represented in Figure 15, using the CC model as a benchmark and evaluating the accuracy of SAME in reproducing the maximum and permanent displacements (Figure 15A,B, respectively). From this figure, the effect of the directional coupling of the plastic response of the abutment in the vertical direction (green circles) is quite evident: when the external loading includes only the vertical component (circles in the lower part of the plots), the differences between the macroelement and the coupled model do not exceed 30% for all the input records and, in particular, the permanent displacements computed with the two methods are very similar (Figure 15B). On the other hand, the simultaneous presence of the vertical and horizontal loads leads to the most marked differences between the two models, for which the macroelement produces lower vertical displacements.

The comparison between the horizontal displacements computed with the two models (blue and red circles) is more satisfactory. In this case, the macroelement predictions are slightly larger or lower than those obtained with the benchmark. On average, the maximum and residual horizontal displacements are moderately underestimated by 10% and 14%, respectively.

7 | CONCLUSIONS

In a modern conception of the soil–structure interaction, the soil–foundation system should be regarded as one of the several members that contribute to the seismic performance of the structure. However, the explicit inclusion of continuous soil elements in a dynamic calculation is quite difficult, as it entails the development of large three-dimensional soil–structure models. Hence, the development of a plasticity-based macroelement is principally aimed at obtaining a concise constitutive behaviour of the soil-foundation system. This element can be inserted in a structural model with a negligible increment in the computational demand, without renouncing to the fundamental aspects of the soil-foundation response, including nonlinear and frequency-dependant features.

Although the soil exhibits a nonlinear behaviour in most loading conditions, and this is reflected by a nonlinear behaviour of the soil–abutment system at the macro scale, a linear description of the system may still be adequate for

low intensities of the seismic motion. However, when the nonlinear behaviour of the structure is modelled explicitly, to account for instance for the irreversible deformation of the bearing system or to consider the nonlinear behaviour of the piers, it is important that the structural nonlinearity be associated with a correspondingly nonlinear behaviour of the soil-foundation system, as the one predicted by the macroelement presented in this paper.

Representing with a macroelement the behaviour of a bridge abutment is more complicated compared to foundations, because in this case the model needs to incorporate the non-symmetric effect of the soil pressure and the strong dynamic interaction with the mass of the approach embankment. Nevertheless, the macroelement for bridge abutments presented in this paper, developed in the framework of multi-surface plasticity and derived from a thermodynamically consistent approach, was seen to be able to reproduce reasonably well the response obtained with a large three-dimensional finite element model, under many combinations of static and dynamic multi-directional loading paths. The simplicity of the calibration procedure, together with its implementation in OpenSees as a multiaxial material, makes it ready to use in any nonlinear analysis aimed at assessing the seismic performance of a bridge.

DATA AVAILABILITY STATEMENT

The data that support the findings of this study are available from the corresponding author upon reasonable request.

ORCID

Davide Noè Gorini https://orcid.org/0000-0001-6673-0071

REFERENCES

1. Gorini DN, Callisto L, Whittle AJ. An inertial macroelement for bridge abutments. *Geotechnique*. 2022;72(3):247-259. doi:10.1680/jgeot.19.P.397
2. Taskari O, Sextos A. Probabilistic assessment of abutment-embankment stiffness and implications in the predicted performance of short bridges. *J Earthq Eng*. 2015;19(5):822-846. doi:10.1080/13632469.2015.1009586
3. Gorini DN, Callisto L, Whittle AJ. Dominant responses of bridge abutments. *Soil Dyn Earthq Eng*. 2021;148:106723. doi:10.1016/j.soildyn.2021.106723
4. Elgamal A, Yan L, Yang Z, Conte JP. Three-dimensional seismic response of Humboldt bay bridge-foundation ground system. *J Struct Eng*. 2008;134(7):1165-1176.
5. Gorini DN, Callisto L. *Springer Lecture Notes in Civil Engineering "Geotechnical Research for Land Protection and Development" (CNRIG2019)* (vol. 40); 2020:565-574. doi:10.1007/978-3-030-21359-6_60
6. Gorini DN, Whittle AJ, Callisto L. Ultimate limit states of bridge abutments. *J Geotech Geoenviron Eng*. 2020;146(7):04020054. doi:10.1061/(ASCE)GT.1943-5606.0002283
7. Gorini DN, Whittle AJ, Callisto L, Ultimate design capacity of bridge abutments. Earthquake Geotechnical Engineering for Protection and Development of Environment and Constructions: *Proceedings of the 7th International Conference on Earthquake Geotechnical Engineering, (ICEGE 2019)* Rome, Italy; 2019:2682-2689. doi:10.1201/9780429031274
8. Roscoe KH, Schofield AN. The stability of short pier foundations on sand. *Br Weld J*. 1956:343-354.
9. Nova R, Montrasio L. Settlements of shallow foundations on sand. *Geotechnique*. 1992;41(2):243-256.
10. Cremer C, Pecker A, Davenne L. Modelling of nonlinear dynamic behaviour of a shallow strip foundation with macro-element. *J Earthquake Eng*. 2002;6(2):175-211.
11. Gorini DN. *Soil-Structure Interaction for Bridge Abutments: Two Complementary Macro-Elements*. Thesis. Sapienza University of Rome, Italy; 2019. https://iris.uniroma1.it/handle/11573/1260972
12. Shamsabadi A, Ashour M, Norris G. Bridge abutment nonlinear force-deflection-capacity prediction or seismic design. *J Geotech Geoenviron Eng*. 2005;131(2):151-161.
13. Shamsabadi A, Rollins KM, Kapuskar M. Nonlinear soil-autment-bridge structure interaction for seismic performance-based design. *J Geotech Geoenviron Eng*. 2007;133(6):707-720.
14. Collins IF, Houlsby GT. Application of thermomechanical principles to the modeling of geotechnical materials. *Proc., R. Soc., Lond. A* 1997;453: 1975-2001.
15. Ziegler H. *An Introduction to Thermomechanics*. Elsevier. ISBN: 9780444598936. 1977.
16. Marchi A, Gallese D, Gorini DN, Franchin P, Callisto L. On the seismic performance of integral abutment bridges: from advanced numerical modelling to a practice-oriented analysis method. *Earthquake Engineering and Structural Dynamics*. 2023;1:164-182. doi:10.1002/eqe.3755

17. Le Pape Y, Sieffert JP. Application of thermodynamics to the global modelling of shallow foundations on frictional material. *Int J Numer Anal Methods Geomech*. 2001;25(14):1377-1408.

18. Houlsby GT, Puzrin AM. *Principles of Hyperplasticity*. Springer; 2006.

19. McKenna F. *Object-Oriented Finite Element Analysis: Frameworks for Analysis, Algorithms and Parallel Computing*. Dissertation. University of California; 1997.

20. McKenna F, Fenves GL, Scott MH, Jeremic B. Open System for Earthquake Engineering Simulation; 2000. http://opensees.berkeley.edu

21. Jamiolkowski M, Lo Presti DCF. *Geotechnical characterization of Holocene and Pleistocene Messina sand and gravel deposits. In* Characterization and Engineering Properties of Natural Soils. Balkema Publishers; 2002: 1087-11120.

22. Fioravante V, Giretti D, Jamiolkowski M, Rocchi GF. Triaxial tests on undisturbed samples of gravelly soils from the Sicilian shore of Messina strait. *Bull Earthq Eng*. 2012;10:1717-1744.

23. Zienkiewicz OC, Shiomi T. Dynamic behavior of saturated porous media: the generalized Biot formulation and its numerical solution. *Int J Numer Analyt Methods Geomech*. 1984;8(1):71-96.

24. Yang Z, Elgamal A, Parra E. A computational model for liquefaction and associated shear deformation. *J Geotech Geoenviron Engng ASCE*. 2003;129(12):1119-1127.

25. Prevost JH. A simple plasticity theory for frictional cohesionless soils. *Soil Dyn Earthquake Eng*. 1985;4(1):9-17.

26. Gallese D. *Soil-Structure Interaction for the Seismic Design of Integral Abutment Bridges: From Advanced Numerical Modelling to Simplified Procedures*. Sapienza University of Rome; 2022.

27. Kotsoglou K, Pantazopoulou S. Bridge-embankment interaction under transverse ground excitation. *Earthq Eng Struct Dyn*. 2007;36(12):1719-1740.

28. Kotsoglou A, Pantazopoulou S. Assessment and modeling of embankment participation in the seismic response of integral abutment bridges. *Bull Earthq Eng*. 2009;7:343-361.

29. Kotsoglou A, Pantazopoulou S. Response simulation and seismic assessment of highway overcrossings. *Earthq Eng Struct Dyn*. 2009;39:991-1013.

30. Stefanidou SP, Sextos AG, Kotsoglou AN, Lesgidis N. Soil-structure interaction effects in analysis of seismic fragility of bridges using an intensity-based ground motion selection procedure. *Eng Struct*. 2017;151:366-380.

31. Dvorkin EN, Bathe KJ. A continuum mechanics based four node shell element for general nonlinear analysis. *Engng Comput (Swansea)*. 1984;1:77-88.

32. Gorini DN, Callisto L. Generalised ultimate loads for piled foundations. *Acta Geotechnica*. 2022;17:2495-2516. doi:10.1007/s11440-021-01386-4

33. McKenna F, Fenves GL. Using the OpenSees Interpreter on Parallel Computers. *Network for Earthquake Engrg Simulations Berkeley, CA*; 2008.

How to cite this article: Gorini DN, Callisto L, Whittle AJ, Sessa S. A multiaxial inertial macroelement for bridge abutments. *Int J Numer Anal Methods Geomech*. 2023;1-24. https://doi.org/10.1002/nag.3493

APPENDIX

Figures A1–A3 show the comparisons between the three-axial dynamic responses of the macroelement and the coupled (CC) soil-abutment model subjected to the three-component force time histories relative to the Tabas, Kocaeli and Iwate earthquakes. Except for the vertical direction, the macroelement response appears in a good agreement with the one of the CC model and reflects the considerations made for the Kobe scenario (see Section 6). Significant displacements occur at the end of the dynamic perturbation, mainly caused by the important amplitudes of the external forces in the horizontal plane, that lead to the development of permanent settlements of the abutment as well, as a consequence of the directional coupling of the plastic response. The frequency content and the amplitudes of the resulting displacement time histories provided by SAME are visibly coherent with the response of the CC model, as a direct effect of the combination of the masses m_i with the dissipative macroelement.
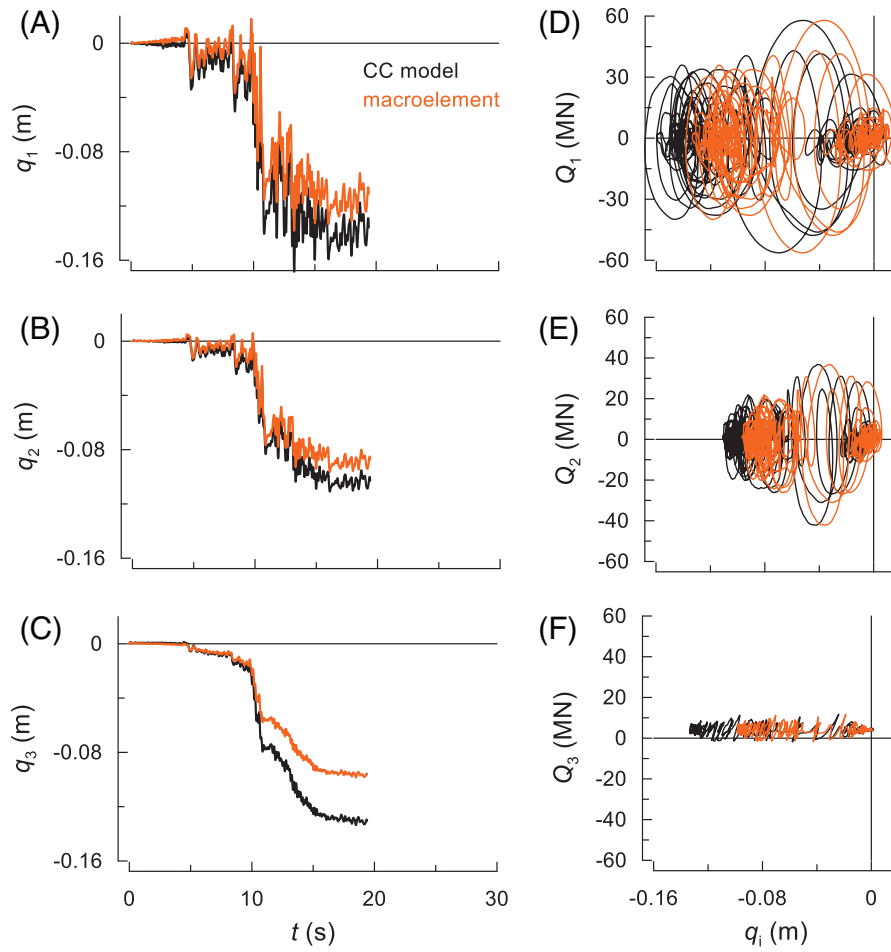
FIGURE A1 Comparison between the responses of the CC model and of the macroelement perturbed by the longitudinal-transverse-vertical force time-histories relative to the Tabas earthquake: a-b-c) time evolution of the displacements q_1, q_2 and q_3, and d-e-f) Q_1-q_1, Q_2-q_2 and Q_3-q_3 relationships
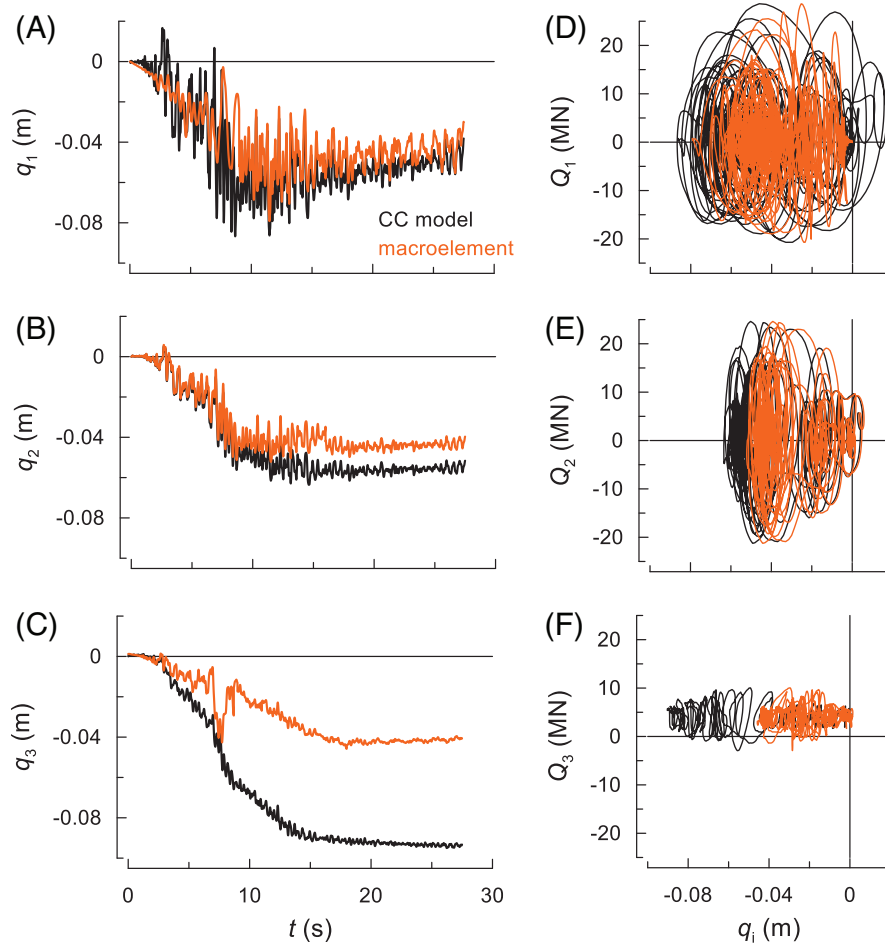
FIGURE A2 Comparison between the responses of the CC model and of the macroelement perturbed by the longitudinal-transverse-vertical force time-histories relative to the Kocaeli earthquake: a-b-c) time evolution of the displacements q_1, q_2 and q_3, and d-e-f) Q_1-q_1, Q_2-q_2 and Q_3-q_3 relationships
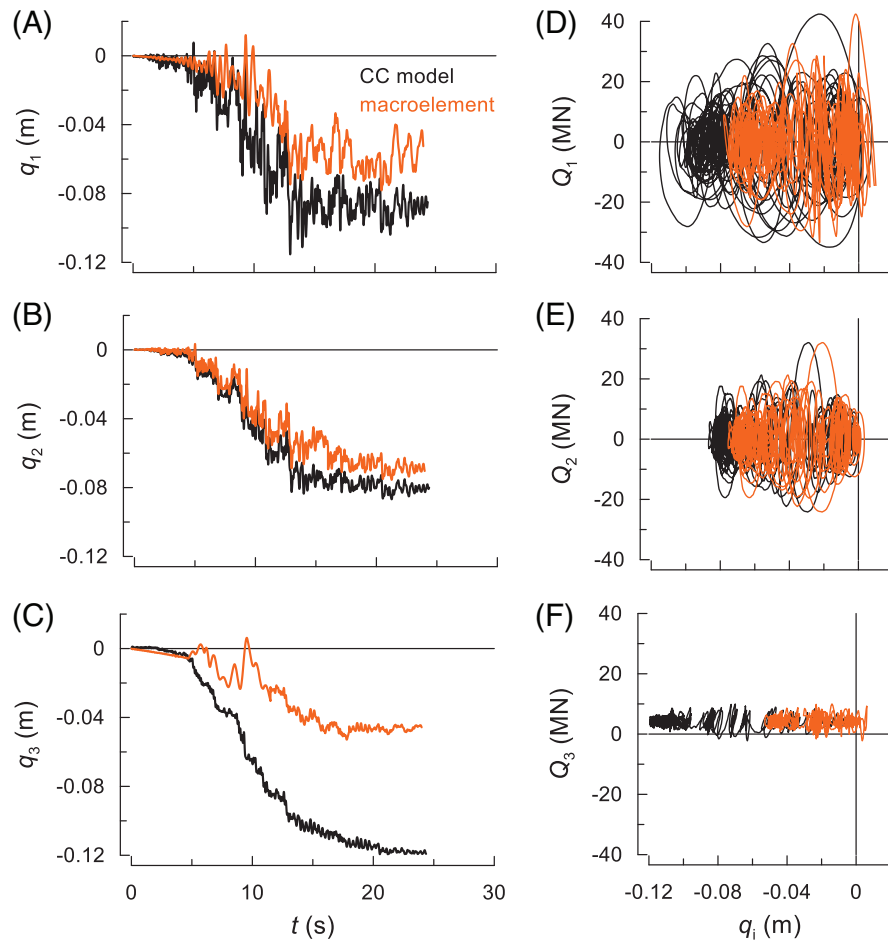
FIGURE A3 Comparison between the responses of the CC model and of the macroelement perturbed by the longitudinal-transverse-vertical force time-histories relative to the Iwate earthquake: a-b-c) time evolution of the displacements q_1, q_2 and q_3, and d-e-f) Q_1-q_1, Q_2-q_2 and Q_3-q_3 relationships